Measurement of the Mitochondrial Membrane Potential and pH Gradient from the Redox Poise of the Hemes of the bc_1 Complex

N. Kim, M. O. Ripple, and R. Springett*
Department of Radiology, Dartmouth Medical School, Hanover, New Hampshire

ABSTRACT   The redox potentials of the hemes of the mitochondrial bc_1 complex are dependent on the proton-motive force due to the energy transduction. This allows the membrane potential and pH gradient components to be calculated from the oxidation state of the hemes measured with multi-wavelength cell spectroscopy. Oxidation states were measured in living RAW 264.7 cells under varying electron flux and membrane potential obtained by a combination of oligomycin and titration with a proton ionophore. A stochastic model of bc_1 turnover was used to confirm that the membrane potential and redox potential of the ubiquinone pool could be measured from the redox poise of the b-hemes under physiological conditions assuming the redox couples are in equilibrium. The pH gradient was then calculated from the difference in redox potentials of cytochrome c and ubiquinone pool using the stochastic model to evaluate the ΔG of the bc_1 complex. The technique allows absolute quantification of the membrane potential, pH gradient, and proton-motive force without the need for genetic manipulation or exogenous compounds.

INTRODUCTION

The bc_1 complex (EC 1.10.2.2) of the mitochondrial electron transport chain transfers electrons from membrane-bound ubiquinol (UQH_2) to intermembrane cytochrome c (Cyt$c$). It catalyzes the net reaction, Reaction 1,

$$UQH_2 + \frac{1}{2}UQ + H_N^+ + Cytc^{3+} \leftrightarrow UQ + 2H_P^+ + \frac{1}{2}UQH_2 + Cytc^{2+},$$
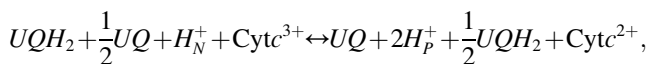
where UQ is ubiquinone, and H_N^+ and H_P^+ refer to protons on the N-side (matrix) and P-side (cytosol) of the membrane, respectively. It operates via the modified Q-cycle (1) in which the two electrons released by ubiquinol oxidation at the Q_o center close to the P-side of the membrane are bifurcated so that one electron is passed along a high potential chain to reduce Cyt$c$, and the other is passed along a low potential chain to reduce ubiquinone at the Q_i center that is located close to the N-side of the membrane (see Fig. 1). The high potential chain consists of an iron-sulfur (Rieske) center and the c_1 heme that is close to the Cyt$c$ docking site. The low potential chain consists of the b_L heme close to the Q_o center and the b_H heme close to the Q_i center. The resulting charge and proton separation results in energy transduction into the proton-motive force (ΔP) that consists of a membrane potential ($\Delta\Psi$) component and proton concentration gradient (ΔH^+, equivalent to Mitchell's $-Z\Delta$pH, the pH gradient expressed in millivolts (2), where $Z = Ln(10)RT/F$). Energy transduction into $\Delta\Psi$ occurs through movement of the electrons between the Q_o and Q_i centers, release of the ubiquinol protons at the Q_o center to the P-side of the membrane and uptake of protons from the N-side of the membrane to reduce ubiquinone at the Q_i

center. Energy transduction into ΔH^+ occurs through uptake and release of protons to and from the Q_i and Q_o centers, respectively. A result of the energy transduction is that the relative redox potentials of the redox centers are dependent on $\Delta\Psi$ and ΔH^+ (Fig. 1). This raises the possibility that $\Delta\Psi$ and ΔH^+ could be quantified from the oxidation state of the hemes of the bc_1 complex measured with multi-wavelength cell spectroscopy. Methods to measure $\Delta\Psi$ in cells use cationic fluorescent dyes that accumulate in the matrix according to the Nernst equation (3). They are nonquantitative (but see Nicholls (4)), nonlinear, and subject to multiple confounding factors. Measurement of matrix and intermembrane space pH in cells requires transfection with targeted pH-sensitive fluorescent proteins (5,6) that require in situ intensity calibration. In contrast, measuring $\Delta\Psi$ and ΔH^+ from the bc_1 complex would enable studies of quantitative cellular bioenergetics without the need for genetic manipulation or exogenous compounds.

The b-hemes are separated in the membrane so that the Gibbs free energy change for electron transfer from b_L to b_H, $\Delta G^{b_L \rightarrow b_H}$, expressed in millivolts, is given by

$$\Delta G^{b_L \rightarrow b_H} = -\left(E_h^{b_H} - E_h^{b_L}\right) + \beta\Delta\Psi, \qquad (1)$$

where $E_h^{b_H}$ and $E_h^{b_L}$ are the redox potentials of b_H and b_L, respectively, β is the fraction of the dielectric distance of the insulating phase between the hemes, and $\Delta\Psi$ is membrane potential. The first term on the right is the energy released on transfer of an electron between redox couples and the second term is the work done against the proton-motive force. The dielectric distance can be approximated by the physical separation of the hemes perpendicular to the membrane expressed as a fraction of the membrane thickness. A disequilibrium, defined as the deviation in ΔG from equilibrium (that is, $-\Delta G$), must be present for
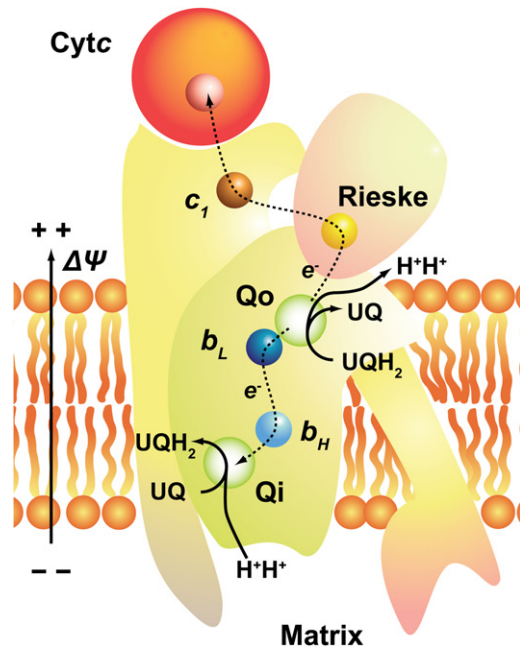
FIGURE 1 Cartoon of the bc_1 complex showing the relative position in the membrane of the redox centers (b_L, b_H, c_1, Rieske), the ubiquinone binding centers (Q_o, Q_i), the bound Cyt, and the high and low potential chain electron pathways.

a net forward flux but the close proximity of the b-hemes leads to a rapid and reversible interheme electron transfer rate and ensures they should remain in close redox equilibrium. In this case, the free energy change can be approximated as zero and $\Delta\Psi$ to be calculated from the redox potentials of the b-hemes that, in turn, can be calculated from their measured oxidation state.

The Gibbs free energy change for electron transfer from b_H to the ubiquinone/ubiquinol pool in the membrane through the Q_i center, $\Delta G^{b_H \to UQ}$, expressed in millivolts per electron transferred, is given by

$$\Delta G^{b_H \to UQ} = -\left(E_h^{UQ} - E_h^{b_H}\right) + \gamma\Delta\Psi, \quad (2)$$

where E_h^{UQ} is the redox potential of the membrane-bound ubiquinone pool with respect to matrix pH and γ is the dielectric depth in the insulating phase of b_H with respect to the matrix. A total of one charge is moved from b_H to the matrix against $\Delta\Psi$ because an electron moves from b_H to Q_i and half of two protons move from the matrix to Q_i. Note that the matrix proton concentration does not appear in Eq. 2 because the protons taken up are substrate protons of the UQ/UQH_2 redox couple and the redox potential of this couple is dependent on the proton concentration in the matrix. Assuming equilibrium, this allows E_h^{UQ} to be calculated from the redox potential of b_H, which can be calculated from its measured oxidation state, and $\Delta\Psi$ calculated from Eq. 1.

The Gibbs free energy of the overall reaction of the bc_1 complex (see Reaction 1, above), expressed in mV per electron transferred from the ubiquinol/ubiquinone pool in the membrane to Cyt$c$ in the intermembrane space, is derived in the Supporting Material and given by

$$\Delta G^{UQ \to Cytc} = -\left(E_h^{Cytc} - E_h^{UQ}\right) + \Delta\Psi + 2\Delta H^+, \quad (3)$$

where E_h^{Cytc} is the redox potential of the Cyt$c$ pool in the intermembrane space. The term in brackets on the right is the energy released when an electron is moved from the UQ pool to the Cyt$c$ pool. This allows ΔH^+ to be calculated from the redox potential of Cyt$c$ (which can be calculated from the measured oxidation state of Cyt$c$, the redox potential of the ubiquinone pool, as calculated from Eq. 2; the membrane potential, as calculated from Eq. 1; and the disequilibrium of the bc_1 complex). Although the bc_1 complex is reversible and works close to equilibrium (7), direct measurements in isolated mitochondria have shown that the disequilibrium is substantial compared to ΔH^+ at high electron flux (8) so that a nonequilibrium model of turnover must be employed to evaluate the extent of the disequilibrium.

Multi-wavelength cell spectroscopy is an emerging technology to measure oxidation changes of the hemes of the electron transport chain from living cells in suspension (9). It uses a linear-combination-of-model-spectra algorithm to calculate the change in oxidation of the hemes from the change in attenuation spectrum. Being an absorption spectroscopy technique, it is strictly quantitative as long as the differential pathlength is known. Although it only measures oxidation changes from baseline, the oxidation states can be back-calculated once the hemes have been fully reduced under anoxic conditions and fully oxidized with an upstream inhibitor (10). The goal of this article is to determine whether $\Delta\Psi$ and ΔP can be quantified in RAW 264.7 cells from the redox poise of the hemes of bc_1 complex under normal physiological conditions and over the dynamic range of electron flux. First, we measure heme oxidation states and bc_1 turnover under baseline conditions and in the physiological range of turnover and membrane potential obtained with a combination of the ATP synthase inhibitor (oligomycin) and proton ionophore (carbonyl cyanide 3-chlorophenylhydrazone, CCCP). We then use a stochastic model of the bc_1 turnover to show that a simple analytical equilibrium model based on Eqs. 1 and 2 can be used to calculate $\Delta\Psi$ and E_h^{UQ} from the oxidation state of b_H and b_L with good accuracy under these conditions. Finally, we use the stochastic model to estimate the disequilibrium necessary to achieve the measured turnover for the measured value of E_h^{Cytc} and derived values of E_h^{UQ} and $\Delta\Psi$ so that ΔH^+ can be estimated from Eq. 3 and ΔP calculated.

MATERIALS AND METHODS

Cell culture

RAW 264.7 mouse macrophage cells were cultured at 37°C in spinner flasks in phenol-red free RPMI medium containing antibiotics/antimycotics

and 10% fetal bovine serum in a 95% air and 5% CO_2 incubator. Cells were spun down at 500g for 5 min and then resuspended at a density of 2.0×10^7 cells/mL in RPMI medium and placed in a custom-built 6 mL chamber that consisted of a 17-mm inside-diameter quartz tube surrounded by a water jacket to maintain the cells at 37°C. The oxygen concentration within the chamber was measured from the fluorescence lifetime of a phosphorescent membrane located at the bottom of the chamber and the top of the chamber was sealed with a stainless-steel plunger. The stir bar was made of glass rather than Teflon (DuPont, Wilmington, DE) and all the seals were made of Viton (DuPont) in accordance with good respirometry practice (11). The chamber could be used in either respirometry or oximetry mode. In respirometry mode, the chamber was sealed and the cellular oxygen consumption measured from the rate of depletion of oxygen. In oximetry mode, the cells were oxygenated and deoxygenated under computer control by exchange of oxygen across 90 mm of narrow-bore silicone tubing immersed in the cell suspension. The tubing always contained 5% CO_2 to maintain intracellular pH.

Spectroscopy and spectral analysis

Heme attenuation spectra and NADH fluorescence spectra were measured with two separate charge-coupled device spectrograph systems working in time-multiplexed mode at 50 Hz using a 6-ms-on, 4-ms-off duty cycle. Contiguous spectra were averaged to give a temporal resolution of 0.5 s. A warm white-light-emitting diode was used for the attenuation spectra illumination that was mounted 10 mm below a bundle of three NA0.37 1-mm optical fibers. One fiber was used for attenuation spectra detection, one for fluorescence spectra detection, and one was coupled to a 365 nm ultraviolet light-emitting diode for fluorescence excitation. The two detection fibers were F-matched onto the slits of two 0.3-mm spectrographs (Triax 320; Horiba, Edison, NJ), each equipped with a 1024 × 128 pixel back-thinned charge-coupled device camera (DV401BV; Andor Technology, South Windsor, CT). The fluorescence data are not reported here. The attenuation spectrograph was equipped with a 600 g/mm grating blazed at 500 nm that provided complete spectra between 508 and 640 nm with a pixel bandpass of 0.16 nm. The slits were set to give a spectral resolution of 1 nm. The spectral analysis and calculation of oxidation states are described in the Supporting Material and in previous reports (10,12).

Redox potentials

The redox potential of Cyt$c$, E_h^{Cytc}, was calculated from the oxidation state using the $n = 1$ Nernst equation assuming a midpoint potential of 260 mV. The redox potential of c_1, $E_h^{c_1}$, was calculated likewise using a midpoint potential of 240 mV.

The redox potential of the ubiquinone pool with respect to the matrix pH is given by

$$E_h^{UQ} \ = \ E_{m,7}^{UQ} + \frac{RT}{2F} Ln\left(\frac{[UQ]\left[H_m^+\right]^2}{[UQH_2]\left[H_7^+\right]^2}\right), \qquad (4)$$

where $E_{m,7}^{UQ}$ is the midpoint potential of the ubiquinone/ubiquinol pool in the membrane at pH 7.0; R is the gas constant; T is absolute temperature (310 K at 37°C); F is the Faraday constant; $[H_m^+]$ is the proton concentration of the matrix; and $[H_7^+]$ is the proton concentration at pH 7.0 (0.1 μM). We define $E_{h,7}^{UQ}$ as the redox potential that a given ubiquinone/ubiquinol ratio would have at pH 7.0, e.g.,

$$E_{h,7}^{UQ} \ = \ E_{m,7}^{UQ} + \frac{RT}{2F} Ln\left(\frac{[UQ]}{[UQH_2]}\right). \qquad (5)$$

The modeling assumes that the cytosol side is at pH 7.0 so that $E_h^{UQ} = E_{h,7}^{UQ} - \Delta H^+$.

Equilibrium measurement of membrane potential

Membrane potential was measured from the redox poise of hemes b_H and b_L assuming Eq. 1 remains at equilibrium. The redox potentials could not be calculated using the Nernst equation because there is substantial redox anti-cooperativity between the hemes, presumably due to simple electrostatic repulsion (13). Instead, a redox cooperativity model (14) using +40 mV and −20 mV for the first-electron midpoint potentials of b_H and b_L, respectively, and −30 mV and −90 mV for the second electron midpoint potentials (13), was employed. To account for the membrane potential, the redox potential of b_L was assumed to be $E_h^{b_H} - \beta\Delta\Psi$. The model was fitted to the oxidation state of b_H and b_L using a Levenberg-Marquardt algorithm with $E_h^{b_H}$ and $\beta\Delta\psi$ as free parameters. The membrane potential is only reported when the reduction state of b_H and b_L is between 10 and 90%, because small errors in reduction state lead to large errors in $\Delta\Psi$ outside this range.

Stochastic model

A stochastic model based on Gillespie's algorithm (15) following Ransac et al. (16), but including the redox anti-cooperativity between the b-hemes and the effect of $\Delta\Psi$ and ΔH^+, was implemented as a native Win32 application in Delphi 2010 (Embarcadero, CA) using mixed object PASCAL and ASSEMBLY language. In brief, the Gillespie algorithm first determines the available partial reactions from a given state. It then chooses the time the enzyme dwells in that state and a partial reaction to be executed. Each choice is based on the available partial reaction rates and a random number. The partial reaction is then executed and the enzyme is moved to the next state from which the process starts again. The algorithm is particularly suited to modeling enzyme turnover because a complex enzyme reaction can be split into multiple simple partial reactions, but a prerequisite is knowledge of the reaction mechanism and the forward and reverse rate constants of the partial reactions.

A single bc_1 complex monomer was modeled to be interacting with thermodynamic pools of intermembrane Cyt$c$, intramembrane ubiquinone, and matrix protons. The partial reactions and their rate constants are listed in Table S1 in the Supporting Material and the midpoint potentials of the redox centers are listed in Table S2. The forward and reverse rate constants were determined from Dutton's Ruler using $\lambda = 0.7$ (17) and previously published distances (16). The forward and reverse rates of electrogenic reactions were determined by weighting the respective rate constants by $e^{-1/2n\delta\Delta\Psi F/RT}$ and $e^{1/2n\delta\Delta\Psi F/RT}$, respectively, where n is the charge and δ is the dielectric distance, as suggested previously (13). The dielectric distance between the matrix and b_H, between b_H and b_L, and between b_L and the intermembrane space was assumed to be 0.25, 0.50 (13), and 0.25, respectively. Anticooperativity between the hemes was modeled by changing their midpoint potentials depending on whether the other heme was oxidized or reduced. The bc_1 is able to precisely bifurcate the electrons into the high and low potential chains, but the mechanism of bifurcation is not known (18,19). The bifurcation mechanism was modeled by only allowing the first and second electron on ubiquinol oxidation at the Q_o center to pass to the Rieske center and b_L, respectively, that is, the leak reactions were not included.

The total concentration of ubiquinone and ubiquinol in the membrane was assumed to be 30 mM (20). The concentration of Cyt$c$ in the intermembrane space was assumed to be 700 μM based on the measured Cyt$c$ concentration of 80 nM in the cell suspension (see Results), the cell suspension containing 1.1% volume by volume of cells at this density (10), and the intermembrane space being 1% of the cell volume.

The stochastic model was used to estimate turnover, occupancy of the ubiquinone binding centers, and oxidation states of the redox centers for given values of E_h^{Cytc}, $E_{h,7}^{UQ}$, $\Delta\Psi$, and ΔH^+. The enzyme was initialized with the ubiquinone centers empty, the redox centers oxidized, and the Rieske center close to Q_o. The system was allowed to evolve for 10^8 partial reactions, which was typically between 5 and 18 s of enzyme time

depending on the starting parameters, and the time-average occupation of the redox centers was logged. Enzyme turnover was measured from the net flux of electrons transferred from the Rieske center to c_1 (that is, the difference between the numbers of forward and reverse partial reactions executed by the simulation divided by the total enzyme time). Computational time was ~30 s per simulation on a six-core 3.2 GHz AMD Phenom II processor.

Statistics

Results are expressed as mean $\pm$ SD ($n = 7$), unless otherwise stated.

RESULTS

Experimental protocol

Fig. 2 shows a representative example of the data collection and experimental protocol. Initially, the cells were maintained in the chamber at an oxygen concentration of 100 μM, a concentration at which the oxidation state of the hemes is independent of the oxygen concentration. A 2-min anoxia was performed by switching the oxygen in the tubing to 0 to fully reduce the hemes, followed by reoxygenation to 100 μM and a 2-min stabilization period. The shaded area in Fig. 2 shows the period when the oxygen concentration was <50 μM. Note that the hemes reduce upon anoxia and return precisely to baseline on reoxygenation.

At time 0, the cells were treated with 100 ng/mL of oligomycin followed by six additions of 75 nM carbonyl cyanide 3-chlorophenylhydrazone (CCCP) separated by 1 min, 1 mM of 3-nitropropionic acid (3-NPA), and finally 1 μM of rotenone. Oligomycin is an ATP synthase inhibitor that blocks proton transport through the ATP synthase, resulting in a rise in ΔP and a decrease in oxygen consumption. CCCP is a proton ionophore that increases the conductivity of the inner mitochondrial membrane to protons. It allows a flux of protons back into the matrix, lowering ΔP, increasing electron flux, and increasing oxygen consumption. Finally, 3-NPA is a complex-II inhibitor and rotenone is a complex-I inhibitor providing the fully oxidized state of the hemes. The signal/noise is lower for the bc_1 hemes compared to Cyt$c$ mainly because of the difference in content: the total content of Cyt$c$, b_H, b_L, and c_1 was 79 $\pm$ 12, 13.6 $\pm$ 1.7, 15.6 $\pm$ 1.9, and 17.7 $\pm$ 2.7 nM, respectively.

The lower graph of Fig. 2 shows $\Delta\Psi$ calculated from the oxidation state of b_H and b_L assuming equilibrium. The data are not shown during the anoxia or after the addition of 3-NPA because errors in the algorithm become large whenever b_H or b_L are highly oxidized or highly reduced. The root mean-square noise on the signal is 7.7 mV, which is large compared to the functional range of $\Delta\Psi$. However, this represents random noise on 0.5-s data collection and the precision can be improved by averaging over an epoch. A 30-s epoch (60 data points) should provide a standard error of the mean of ≈ 1 mV, and this is borne out by averages over 30-s epochs from the baseline, which were 159.8, 158.4, 158.9, 160.4, and 159.3 mV.
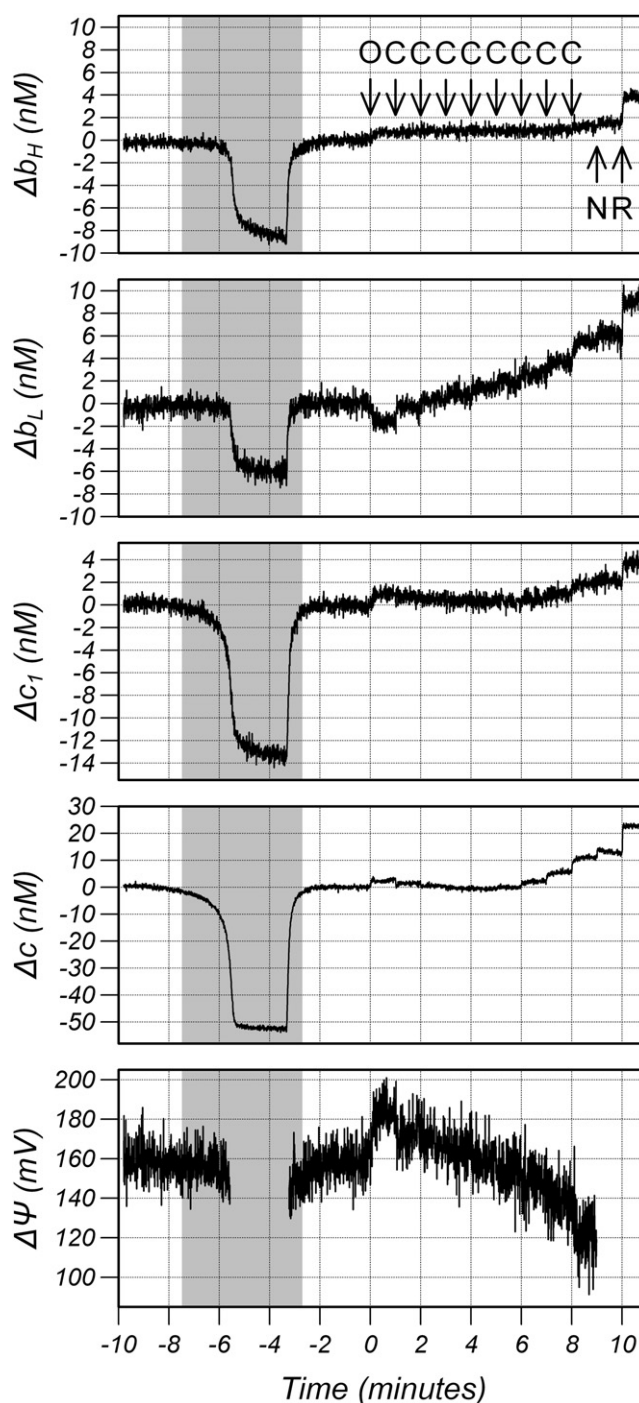

FIGURE 2 Oxidation changes in b_H, b_L, c_1, and Cyt$c$ and $\Delta\Psi$ during the experimental protocol <50 μM. (*Arrows*) Additions to the chamber. (*O*) 5 μg/mL oligomycin, (*C*) 75 nM CCCP, (*N*) 1 mM 3-NPA, and (*R*) 1 μM Rotenone. The hemes were assumed to be fully oxidized after rotenone.

Oxidation states

Paired experiments with cells from the same culture were carried out with the chamber in respirometry mode so that cellular oxygen consumption (VcO_2) could be measured under the same conditions. A separate study using cyanide

to inhibit mitochondrial oxygen consumption (VmO_2) and so separate the contributions of mitochondrial and nonmitochondrial oxygen consumption to VcO_2 was carried out and it was found that nonmitochondrial oxygen consumption is $9.0 \pm 1.3\%$ of baseline (mean $\pm$ SD, $n = 6$). Therefore, VmO_2 at baseline, after oligomycin and after CCCP, was determined by subtracting 9% of the baseline VcO_2 from the measured VcO_2. The results are displayed in the top panel of Fig. 3 along with the oxidation state of the b-hemes (*middle panel*) and the c-hemes (*lower panel*).

Oligomycin decreased VmO_2 to 5.5 ± 0.5 μM/min and subsequent additions of CCCP increased VmO_2 to 48.2 ± 6.5 μM/min, which was an 8.8-fold increase. Pilot studies had shown VmO_2 decreases with at higher CCCP concentrations and VmO_2 was maximal at 525 nM of CCCP in two of the seven studies.

The baseline oxidation state of b_H, b_L, c_1, and Cyt$c$ were 66.2 ± 1.6, 41.3 ± 1.4, 78.5 ± 1.6, and $68.6 \pm 1.6\%$, respectively. The difference in oxidation states between c_1 and Cyt$c$ could be mostly accounted for in their difference in midpoint potential assuming equilibrium. Oligomycin resulted in a $\approx 5\%$ oxidation in b_H, c_1, and Cyt$c$ and a $\approx 10\%$ reduction in b_L. Addition of CCCP up to 300 nM

caused a small reduction in c_1 and Cyt$c$ to slightly below baseline values and then higher concentrations caused an oxidation to above the oligomycin values. The b-hemes oxidized with increasing CCCP but the oxidation in b_H was small ($<6\%$), whereas the oxidation in b_L was substantial ($>45\%$). Pilot studies showed that even higher concentrations of CCCP resulted in a profound oxidation of all the hemes of the electron transport chain concomitant with the decrease in VmO_2.

Redox potentials

Fig. 4 shows turnover number of the bc_1 complex, redox potentials of Cyt$c$ and ubiquinone, $\Delta\Psi$, and the redox span (ΔE_s) of the bc_1 complex. The redox span is the difference in redox potentials of Cyt$c$ and UQ/UQH_2 and the term in brackets in Eq. 2. Baseline turnover was $92 \pm 13e$/s and decreased to $24 \pm 2e$/s after oligomycin and increased to a maximum of $206 \pm 28e$/s after 600 nM of CCCP. Baseline $\Delta\Psi$ was 155 ± 2 mV and increased to 180 ± 3 mV after oligomycin and decreased to a minimum of 121 ± 11 mV after 600 nM of CCCP. The redox potential of Cyt$c$ remained remarkably constant, and only varied between
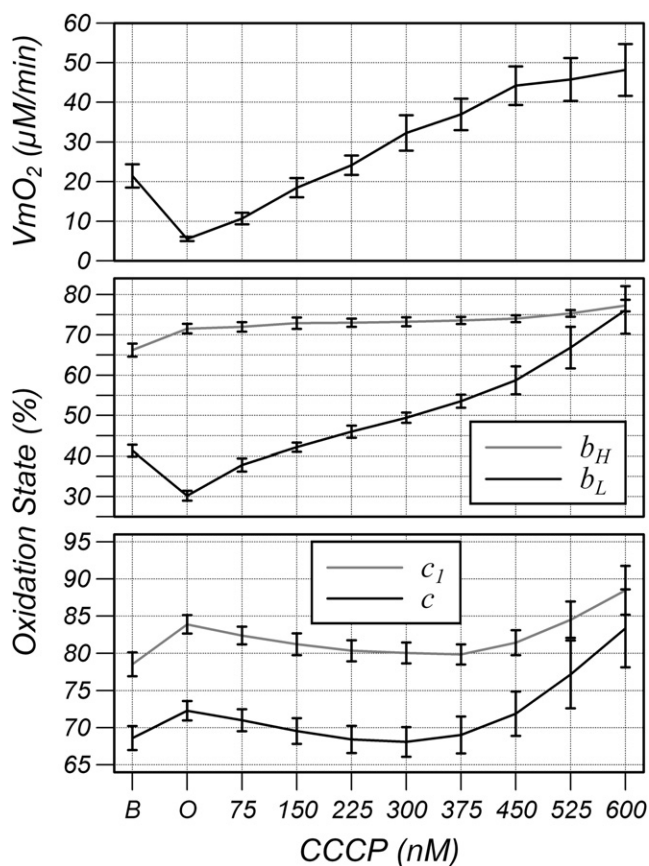

FIGURE 3 Mitochondrial oxygen consumption and oxidation state of b_H, b_L, c_1, and Cyt$c$ under baseline conditions (*B*), after oligomycin (*O*) and subsequent addition of CCCP.
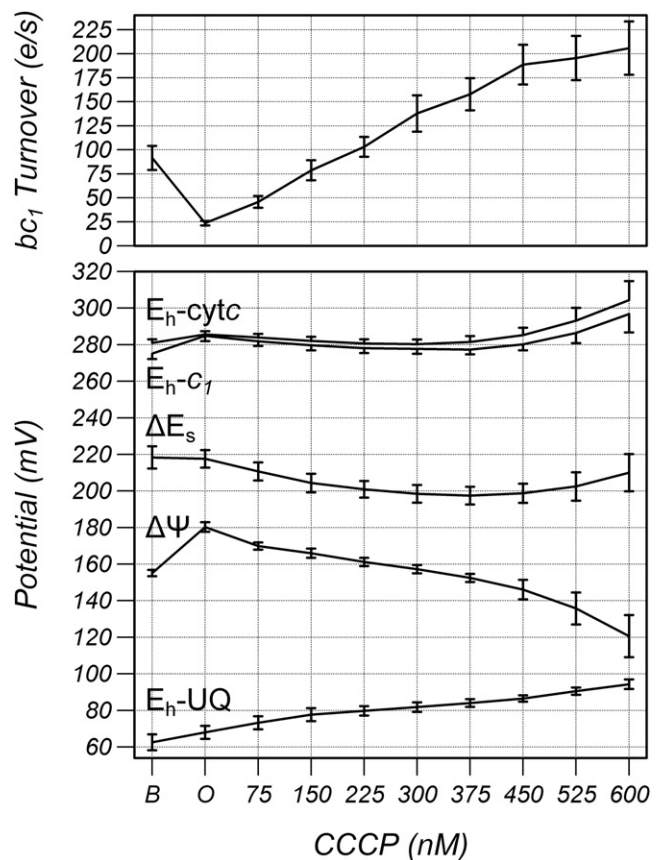
FIGURE 4 The bc_1 turnover, redox potentials of Cyt$c$, c_1, and UQ, bc_1 redox span, and $\Delta\Psi$ under baseline conditions (*B*), after oligomycin (*O*) and subsequent addition of CCCP.

280 and 285 mV except at the highest two concentrations of CCCP.

Stochastic modeling

To compare the results of the stochastic model with published data, the experimental protocol of Sun and Trumpower (21) was modeled in which the reaction of isolated bovine heart bc_1 complex was followed in the presence of 50 μM of decyl-ubiquinol and 40 μM of oxidized Cyt$c$ at pH 7.4. Enzyme turnover was simulated at the concentrations of reactants and products that would be present as the enzyme transferred electrons from the ubiquinol to Cyt$c$ pools. The model predicted a maximum turnover of 271e/s when the enzyme had consumed 4 μM of UQH$_2$, which compares favorably with the measured turnover of 355e/s (21).

To justify using an analytical equilibrium model to estimate $\Delta\Psi$ and E_h^{UQ} from the oxidation state of the hemes using Eqs. 1 and 2, stochastic simulations were carried out to estimate the turnover and oxidation state of b_H and b_L using parameters comparable to those found in RAW cells. The values $\Delta\Psi$ and E_h^{UQ} were then estimated from the oxidation state of the hemes using the equilibrium model and compared to the known values used to run the simula-

tion. Fig. 5 shows an example of the results. Simulations were carried out with $E_h^{Cytc} = 285$ mV, $\Delta H^+ = 20$ mV, and $E_{h,7}^{UQ}$ varied between 0 and 180 mV in steps of 5 mV (plotted on the x axis) at $\Delta\Psi = 120$ mV (*left graphs*), $\Delta\Psi = 150$ mV (*center graphs*), and $\Delta\Psi = 180$ mV (*right graphs*). The shaded regions represent the range of $E_{h,7}^{UQ}$ in which the disequilibrium of the reaction was between 0 and 60 mV. The turnover is shown in the upper graphs and the values are compatible with the physiological data and the assumption that the bc_1 complex works close to equilibrium (e.g., at $\Delta\Psi = 120$, 150, and 180 mV, the observed turnover (Fig. 3) is ≈ 220, 150, and 25 e/s, respectively, which would require a disequilibrium of <30 mV, <15 mV, and <5 mV, respectively). The oxidation state of b_H and b_L are plotted in the second row of graphs. The effective midpoint potentials of b_H and b_L are the same when $\Delta\Psi = 120$ mV and both hemes would be expected to have the same oxidation state assuming they remain in equilibrium, as is found. Heme b_L becomes increasingly more reduced with respect to b_H with increasing $\Delta\Psi$, as would be expected if the hemes remained in redox equilibrium.

The difference between the values of $\Delta\Psi$ and E_h^{UQ} estimated from the oxidation state of b_H and b_L using the equilibrium model and the values used in the simulation are plotted in the lower graphs of Fig. 5. Under all conditions,
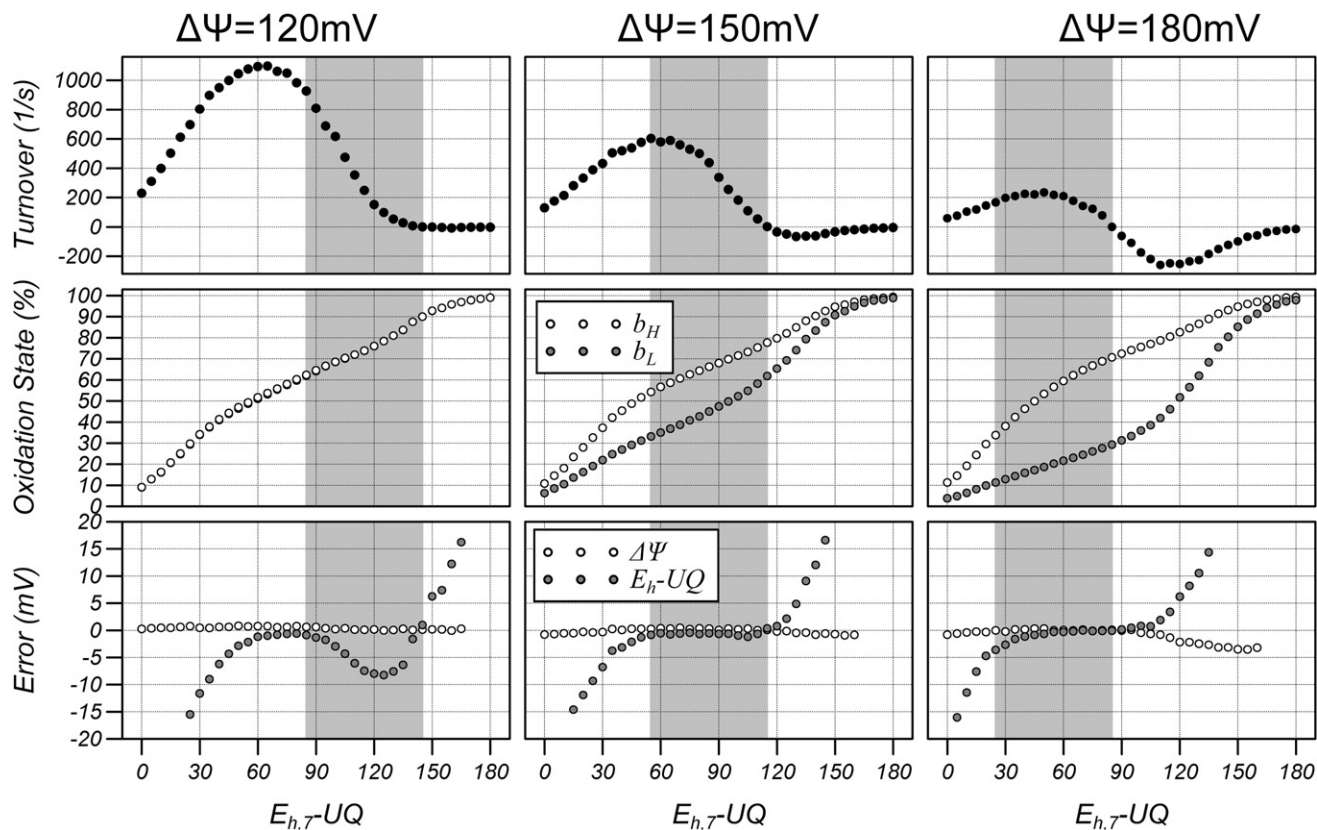

FIGURE 5 Stochastic model estimations of bc_1 turnover (*upper panels*), oxidation states of b_H and b_L (*middle panels*), and the difference between $\Delta\Psi$ and E_h^{UQ} used the model and calculated from the oxidation state of the hemes assuming equilibrium (*lower panels*) as a function of $E_{h,7}^{UQ}$ for $\Delta\Psi = 120$ mV (*left panels*), 150 mV (*center panels*), and 180 mV (*right panels*). The values E_h^{Cytc} and ΔH^+ were set to 285 and 20 mV, respectively.

the estimated value of $\Delta\Psi$ was <1 mV different from the value used in the simulation except at high $\Delta\Psi$ under conditions where the bc_1 complex is running backward. Even then, the maximum error is <4 mV. The estimated value of E_h^{UQ} was similarly very good at high $\Delta\Psi$ in the range of disequilibrium that could be expected where the maximum error was 3.6 mV at $\Delta\Psi = 180$ mV and $\Delta G = -60$ mV. At 120 mV, the accuracy of the estimated E_h^{UQ} and the greatest error was 8.3 mV at a ΔG of -20 mV. However, only half of this error propagates into ΔH^+ when using Eq. 2 so that ΔH^+ should be accurate to <2 mV at high $\Delta\Psi$ and <5 mV at lower $\Delta\Psi$.

Estimation of ΔH^+

The operating disequilibrium of the bc_1 complex was estimated by performing stochastic simulations to determine the degree of disequilibrium necessary to match the observed turnover. Simulations were carried out at the observed values of E_h^{Cytc}, E_h^{UQ}, and $\Delta\Psi$ shown in Fig. 4 at different values of ΔH^+ to vary the disequilibrium of the reaction. Fig. 6 shows the difference in turnover between the simulation and the measured turnover as a function of disequilibrium for parameters sets measured after oligomycin, 150, 300, 450, and 600 nM of CCCP. The difference in turnover is plotted for clarity as the curves for 0, 150, 300, and 450 nM of CCCP, and under baseline conditions, overlay each other when the simulated turnover is plotted but also because the disequilibrium can easily estimated from where the curves cross the $\Delta_{Turnover} = 0$ line. The disequilibrium was estimated for each experimental point in the seven datasets and presented in Fig. 7 along with the measured difference in the redox span and $\Delta\Psi$ that, according to
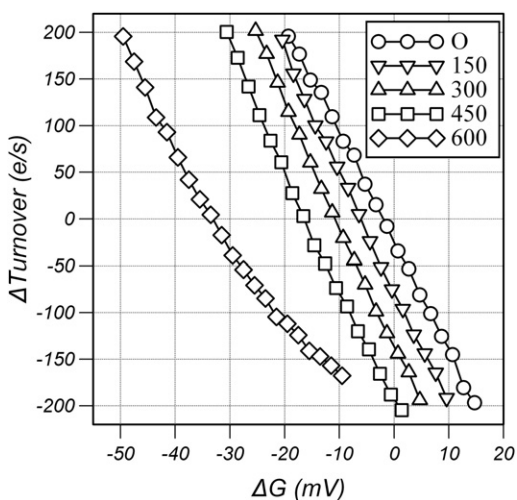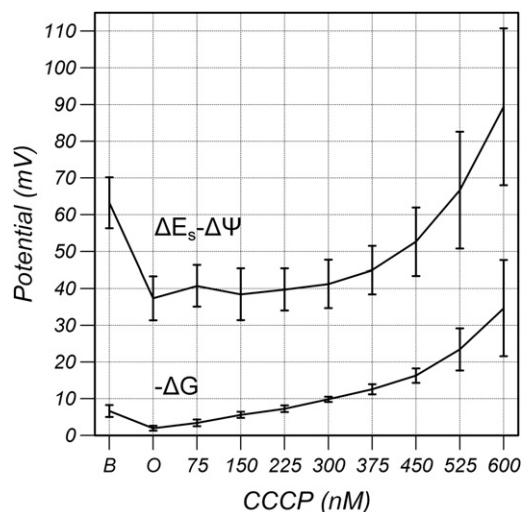
FIGURE 7 Disequilibrium of the bc_1 complex calculated from the stochastic simulations compared to the difference between the redox span of the bc_1 complex and $\Delta\Psi$, which is equal to $2\Delta H^+ + \Delta G$ under baseline conditions (B), after oligomycin (O) and subsequent addition of CCCP.

Eq. 3, is equal to $2\Delta H^+ - \Delta G$ such that the difference of the two curves is equal to $2\Delta H^+$.

The baseline disequilibrium was 7 ± 2 mV and fell to 2 ± 1 mV after oligomycin and then increased with increasing turnover to 35 ± 13 mV after 600 nM of CCCP. The calculated values of ΔH^+, $\Delta\Psi$, and ΔP are shown in Fig. 8. Baseline ΔH^+ was 28 ± 3 mV; this decreased to 18 ± 3 mV after oligomycin, trended downwards to a minimum of 16 ± 3 mV at 300 nM of CCCP, and then increased to 27 ± 5 mV after 600 nM of CCCP. Baseline ΔP was 184 ± 2 mV, increased to 198 ± 2 mV, and declined to 148 ± 7 mV after 600 nM of CCCP.

DISCUSSION

The stochastic simulations confirmed that the b-hemes of the bc_1 complex operate very close to equilibrium under the full dynamic range of electron flux found in the RAW 264.7 mouse macrophage cells so that the membrane potential can be measured from their oxidation state with millivolt accuracy. The model also predicts that ΔH^+ can be measured from the equilibrium poise of the enzyme using the redox state of b_H as a surrogate for the redox potential of the ubiquinone pool. Furthermore, the oxidation state of the b-hemes can be measured with sufficient signal/noise for the calculation of these parameters with millivolt precision. The accuracy of the calculated $\Delta\Psi$ will depend on the accuracy of the measurement of the oxidation state of the b-hemes, which in turn depends on the ability to fully reduce and fully oxidize them, and the accuracy of the midpoint potentials used in the redox cooperativity model. The accuracy of the calculated ΔH^+ also depends on the accuracy of the measurement of redox potential of Cyt$c$ and the ability

FIGURE 6 Difference between the measured and simulated bc_1 turnover as a function of ΔG using values of bc_1 turnover, E_h^{Cytc}, E_h^{UQ}, and $\Delta\Psi$ from oligomycin-inhibited cells (O) and after addition of 150, 300, 450, and 600 nM of CCCP. The value ΔG was varied in the simulation by varying ΔH^+.
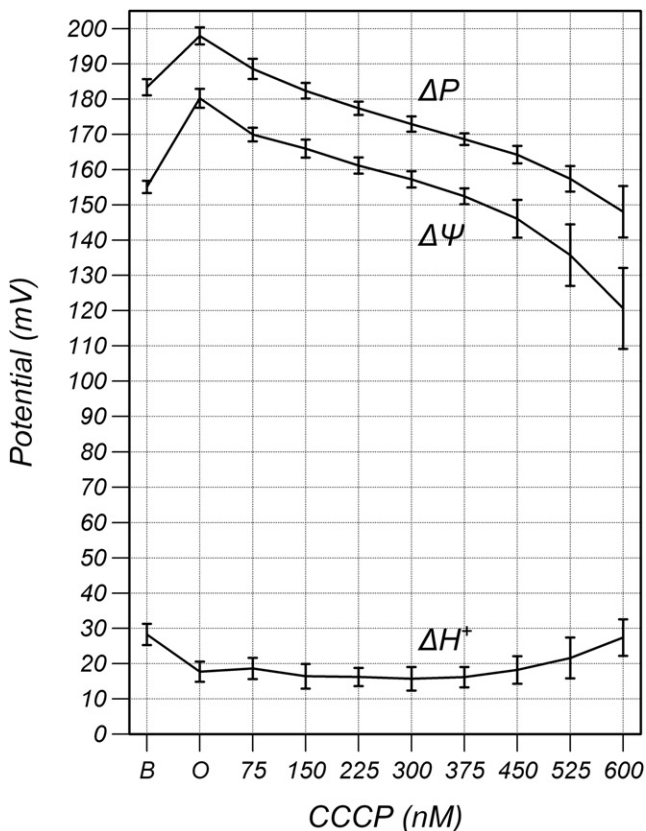
FIGURE 8   Values ΔP, $\Delta \Psi$, and ΔH^+ under baseline conditions (B), after oligomycin (O) and subsequent addition of CCCP.

of the stochastic model to estimate the disequilibrium for the given turnover conditions. Validation of the measurements is hampered by the lack of a gold-standard to measure $\Delta \Psi$.

The mitochondrial membrane potential can be measured in isolated mitochondria with a tetraphenyl phosphonium (TPP^+) electrode (22), which provides a continuous time trace, and both $\Delta \Psi$ and ΔH^+ can be measured simultaneously from aliquots using radioactive tracers (^{86}Rb for $\Delta \Psi$ and the membrane-permeant weak acid ^{3}H-acetate and weak base ^{14}C-methylamine for ΔH^+) in the presence of the potassium ionophore, valinomycin, to make the inner membrane permeant to rubidium (23). Using this method, the maximum ΔP was found to be ≈ 220 mV in both state-4 respiration and by reversal of the ATP synthase, and the minimum ΔP under state-3 respiration was 173 mV. The contribution of $\Delta \Psi$ and ΔH^+ to ΔP was split 153:66 mV in state 4 and 137:38 mV in state 3. However, the valinomycin tends to redistribute the components of ΔP to favor higher ΔH^+ and lower $\Delta \Psi$, even in low potassium media. In contrast, the matrix and cytosol contains 120 mM of potassium (24) and similar concentrations of chloride and millimolar concentrations of sodium, which are maintained far from their Nernst equilibrium by the high impermeability of the inner membrane and by electroneutral ionic antiporters (25,26). Therefore, isolated mito-

chondrial studies only weakly inform on the magnitude of ΔP and its distribution into $\Delta \Psi$ and ΔH^+ when mitochondria are in their physiological environment within cells.

Methods to measure $\Delta \Psi$ in cells rely on the use of membrane-permeant, cationic fluorescent probes such as tetramethyl rhodamine ethyl ester (TMRE), tetramethyl rhodamine methyl ester (TMRM) (27), and JC1, which accumulate in the mitochondrial matrix according to the Nernst equation (see Nicholls and Ward (3) for a review). At high concentrations, the probes aggregate, which quenches the fluorescence for TMRE and TMRM so that TMRM must be used at a concentration of <5 nM (4). A major confounding error will occur if the indicator enters the quenching regime because then a small decline in $\Delta \Psi$ will result in an increase in fluorescence, whereas a collapse in $\Delta \Psi$ obtained by adding a high concentration of a proton ionophore, which is often used as a control, will cause a decrease in fluorescence. Thus, even the direction change in $\Delta \Psi$ may be misrepresented if great care is not taken. The JC1 aggregates fluoresce at a different wavelength compared to the free fluorophore allowing for a ratiometric measurement but the aggregates are slow to disassociate (3).

All the indicators are sensitive to matrix volume, which is a particular problem in apoptotic studies due to cristae remodeling after caspase activation (28), and also the plasma membrane potential, which causes accumulation of the indicator in the cytosol, but which is rarely measured in nonneuronal cell lines. The membrane potential can be deconvoluted and quantified from the fluorescence signal if the rate constants for equilibration across the plasma and mitochondrial membrane are known, if the relative matrix volume is known, if the plasma membrane potential is known, and if nonspecific binding is assumed negligible (4), but this is very rarely carried out. In contrast, measurement of $\Delta \Psi$ from the b-hemes is entirely independent of the plasma-membrane potential and the matrix volume, as it only depends on the electric field within the inner mitochondrial membrane in which the bc_1 complex is embedded. Furthermore, the theoretical temporal resolution, based on the intraheme rate constants, is on the microsecond scale, although the signal/noise limits the measurements to tens of seconds to obtain millivolt precision.

Under baseline conditions, $\Delta \Psi$, ΔH^+, and ΔP were measured to be 155 ± 2, 28 ± 3, and 183 ± 2 mV, respectively, which compares extremely well with the estimated normal values in cells of 150, 30, and 180 mV, respectively (3,4). Oligomycin caused an increase in $\Delta \Psi$ to 180 ± 3 mV but a decrease in ΔH^+ to 18 ± 3 mV resulting in a ΔP of 198 ± 2 mV. The higher ΔP in mitochondria under state-4 respiration compared to the oligomycin-inhibited cells is not surprising, because the mitochondria preparation uses an artificial electron donor system (glutamate and malate operating through the malate-aspartate shuttle system) that is able to fully reduce NADH in state-4 (29). This drives the ETC to generate a higher ΔP than in cells in which

the electron source originates from the TCA cycle. If oligomycin simply caused a transient net efflux of protons, then both $\Delta\Psi$ and ΔH^+ would be expected to increase and the ratio of the increase should depend on the relative capacitance of the inner mitochondrial membrane and the matrix pH buffering capacity. But in the milieu of the cell, there will be a reequilibration of ions, weak acids, and weak bases across the inner membrane that could redistribute the contribution of $\Delta\Psi$ and ΔH^+ to ΔP. In particular, an accumulation of a weak base or inorganic phosphate (the latter being cotransported into the matrix with a proton by the phosphate symporter) would tend to decrease ΔH^+, as occurs on addition of phosphate to isolated mitochondria (23).

Addition of CCCP to the oligomycin-inhibited cells decreases ΔP and $\Delta\Psi$, as would be expected. The value ΔH^+ decreased at concentrations of CCCP below 375 nM, broadly consistent with a $\approx 90{:}10\%$ distribution of ΔP into $\Delta\Psi/\Delta H^+$, but ΔH^+ increased at higher concentration of CCCP. The value ΔP could not be measured at much higher concentrations of CCCP that would collapse ΔP completely because, under these conditions, all the hemes of the electron transport chain become highly oxidized, making the estimation of their redox potentials error-prone. The increase in ΔH^+ is thermodynamically possible as ΔP continually decreases with increasing CCCP, but the apparent increase in ΔH^+ could be the result of an underestimation of the disequilibrium of the bc_1 complex by the stochastic model. The disequilibrium of the bc_1 complex has been measured in isolated mitochondria and found to be similar to the values calculated by the stochastic simulations (8). The disequilibrium was ≈ 6 mV in oligomycin-inhibited mitochondria compared to 2 mV in the simulations, and increased to ≈ 48 mV in the mitochondria at high flux obtained with a proton ionophore, compared to 35 mV in simulations. However, the results are not precisely comparable, because the flux was measured in terms of oxygen consumption per mg of protein in the mitochondrial study rather than turnover of the bc_1 complex. Furthermore, the electron donor in the mitochondrial studies was succinate; this may have led to a higher maximum turnover, and the respiratory control ratio was <4 in the mitochondria compared to 8.8 in the cells that may also have made the oligomycin turnover higher.

The calculation of ΔH^+ from Eq. 3 depends directly on the midpoint potential of Cyt$c$ used in the calculation of its redox potential. The midpoint potential of isolated Cyt$c$ varies between 270 and 290 mV depending on ionic strength and concentration of chloride and phosphate (30), and has been measured to be 230 mV in isolated mitochondria (31). There are reports of increases in midpoint potential on Cyt$c$ binding to artificial membranes (32) although studies have shown that Cyt$c$ diffuses in three dimensions in the mitochondria intermembrane space at physiological ionic strength (33–35), and decreases from 282 to 252 mV in the presence of increasing concentration of cytOx (36).

All reports observe that Cyt$c$ titrates with an $n = 1$ Nernst function so that only the error in the midpoint potential would affect the calculation of ΔH^+ and would result in an offset of half the magnitude being added to ΔH^+. In support of our use of 260 mV, it was found that the difference in midpoint potential between Cyt$c$ and c_1 varied by only 8 mV over the dynamic range of turnover, and the stochastic simulations predict that a component of this can be attributed to the disequilibrium between Cyt$c$ and c_1.

CONCLUSION

In this article, we have shown that the $\Delta\Psi$ can be measured from the redox poise of the b-hemes of the bc_1 complex with millivolt precision. Furthermore, the stochastic simulations predict that the redox potential of the ubiquinone pool can be calculated from the redox potential of b_H with millivolt accuracy except at low membrane potential when turnover is very high. This allows ΔH^+ to be calculated from the difference in the redox potentials of the Cyt$c$ and ubiquinone pools. Application of this technique could make quantitative cellular bioenergetics possible and lead to a more precise understanding of the function of the mitochondrial electron transport chain.

SUPPORTING MATERIAL

Stochastic model, spectroscopy, measurement of $\Delta\Psi$ and ΔH^+, derivation of Eq. 3, two tables, a figure, and references (37–40) are available at http://www.biophysj.org/biophysj/supplemental/S0006-3495(12)00202-0.

REFERENCES

1. Crofts, A. R., S. W. Meinhardt, …, M. Snozzi. 1983. The role of the quinone pool in the cyclic electron-transfer chain of *Rhodopseudomonas sphaeroides*: a modified *q*-cycle mechanism. *Biochim. Biophys. Acta.* 723:202–218.

2. Mitchell, P. 1979. Keilin's respiratory chain concept and its chemiosmotic consequences. *Science.* 206:1148–1159.

3. Nicholls, D. G., and M. W. Ward. 2000. Mitochondrial membrane potential and neuronal glutamate excitotoxicity: mortality and millivolts. *Trends Neurosci.* 23:166–174.

4. Nicholls, D. G. 2006. Simultaneous monitoring of ionophore- and inhibitor-mediated plasma and mitochondrial membrane potential changes in cultured neurons. *J. Biol. Chem.* 281:14864–14874.

5. Llopis, J., J. M. McCaffery, …, R. Y. Tsien. 1998. Measurement of cytosolic, mitochondrial, and Golgi pH in single living cells with green fluorescent proteins. *Proc. Natl. Acad. Sci. U S A.* 95:6803–6808.

6. Azarias, G., H. Perreten, …, J. Y. Chatton. 2011. Glutamate transport decreases mitochondrial pH and modulates oxidative metabolism in astrocytes. *J. Neurosci.* 31:3550–3559.

7. Osyczka, A., C. C. Moser, …, P. L. Dutton. 2004. Reversible redox energy coupling in electron transfer chains. *Nature.* 427:607–612.

8. Brown, G. C., and M. D. Brand. 1985. Thermodynamic control of electron flux through mitochondrial cytochrome bc_1 complex. *Biochem. J.* 225:399–405.

9. Hollis, V. S., M. Palacios-Callender, ..., S. Moncada. 2003. Monitoring cytochrome redox changes in the mitochondria of intact cells using multi-wavelength visible light spectroscopy. *Biochim. Biophys. Acta.* 1607:191–202.

10. Ripple, M. O., M. Abajian, and R. Springett. 2010. Cytochrome c is rapidly reduced in the cytosol after mitochondrial outer membrane permeabilization. *Apoptosis.* 15:563–573.

11. Haller, T., M. Ortner, and E. Gnaiger. 1994. A respirometer for investigating oxidative cell metabolism: toward optimization of respiratory studies. *Anal. Biochem.* 218:338–342.

12. Kim, N., M. O. Ripple, and R. Springett. 2011. Spectral components of the α-band of cytochrome oxidase. *Biochim. Biophys. Acta.* 1807:779–787.

13. Shinkarev, V. P., A. R. Crofts, and C. A. Wraight. 2001. The electric field generated by photosynthetic reaction center induces rapid reversed electron transfer in the bc_1 complex. *Biochemistry.* 40:12584–12590.

14. Hendler, R. W., and H. V. Westerhoff. 1992. Redox interactions in cytochrome c oxidase: from the "neoclassical" toward "modern" models. *Biophys. J.* 63:1586–1604.

15. Gillespie, D. T. 1977. Exact stochastic simulation of coupled chemical-reactions. *J. Phys. Chem.* 81:2340–2361.

16. Ransac, S., N. Parisey, and J. P. Mazat. 2008. The loneliness of the electrons in the bc_1 complex. *Biochim. Biophys. Acta.* 1777:1053–1059.

17. Moser, C. C., T. A. Farid, ..., P. L. Dutton. 2006. Electron tunneling chains of mitochondria. *Biochim. Biophys. Acta.* 1757:1096–1109.

18. Ransac, S., and J. P. Mazat. 2010. How does antimycin inhibit the bc_1 complex? A part-time twin. *Biochim. Biophys. Acta.* 1797:1849–1857.

19. Darrouzet, E., C. C. Moser, ..., F. Daldal. 2001. Large scale domain movement in cytochrome bc_1: a new device for electron transfer in proteins. *Trends Biochem. Sci.* 26:445–451.

20. Ding, H., C. C. Moser, ..., P. L. Dutton. 1995. Ubiquinone pair in the Q_o site central to the primary energy conversion reactions of cytochrome bc_1 complex. *Biochemistry.* 34:15979–15996.

21. Sun, J., and B. L. Trumpower. 2003. Superoxide anion generation by the cytochrome bc_1 complex. *Arch. Biochem. Biophys.* 419:198–206.

22. Kamo, N., M. Muratsugu, ..., Y. Kobatake. 1979. Membrane potential of mitochondria measured with an electrode sensitive to tetraphenyl phosphonium and relationship between proton electrochemical potential and phosphorylation potential in steady state. *J. Membr. Biol.* 49:105–121.

23. Nicholls, D. G. 1974. The influence of respiration and ATP hydrolysis on the proton-electrochemical gradient across the inner membrane of rat-liver mitochondria as determined by ion distribution. *Eur. J. Biochem.* 50:305–315.

24. Nicholls, D. G. 2005. Commentary on: 'old and new data, new issues: the mitochondrial Deltapsi' by H. Tedeschi. *Biochim. Biophys. Acta.* 1710:63–66.

25. Garlid, K. D., and P. Paucek. 2003. Mitochondrial potassium transport: the K^+ cycle. *Biochim. Biophys. Acta.* 1606:23–41.

26. Bernardi, P. 1999. Mitochondrial transport of cations: channels, exchangers, and permeability transition. *Physiol. Rev.* 79:1127–1155.

27. Scaduto, Jr., R. C., and L. W. Grotyohann. 1999. Measurement of mitochondrial membrane potential using fluorescent rhodamine derivatives. *Biophys. J.* 76:469–477.

28. Sun, M. G., J. Williams, ..., T. G. Frey. 2007. Correlated three-dimensional light and electron microscopy reveals transformation of mitochondria during apoptosis. *Nat. Cell Biol.* 9:1057–1065.

29. Chance, B., and G. R. Williams. 1955. Respiratory enzymes in oxidative phosphorylation. III. The steady state. *J. Biol. Chem.* 217:409–427.

30. Gopal, D., G. S. Wilson, ..., M. A. Cusanovich. 1988. Cytochrome c: ion binding and redox properties. Studies on ferri and ferro forms of horse, bovine, and tuna cytochrome c. *J. Biol. Chem.* 263:11652–11656.

31. Dutton, P. L., D. F. Wilson, and C. P. Lee. 1970. Oxidation-reduction potentials of cytochromes in mitochondria. *Biochemistry.* 9:5077–5082.

32. Salamon, Z., and G. Tollin. 1997. Interaction of horse heart cytochrome c with lipid bilayer membranes: effects on redox potentials. *J. Bioenerg. Biomembr.* 29:211–221.

33. Gupte, S. S., and C. R. Hackenbrock. 1988. The role of cytochrome c diffusion in mitochondrial electron transport. *J. Biol. Chem.* 263:5248–5253.

34. Gupte, S. S., and C. R. Hackenbrock. 1988. Multidimensional diffusion modes and collision frequencies of cytochrome c with its redox partners. *J. Biol. Chem.* 263:5241–5247.

35. Cortese, J. D., and C. R. Hackenbrock. 1993. Motional dynamics of functional cytochrome c delivered by low pH fusion into the intermembrane space of intact mitochondria. *Biochim. Biophys. Acta.* 1142:194–202.

36. Kojima, N., and G. Palmer. 1983. Further characterization of the potentiometric behavior of cytochrome oxidase. Cytochrome α stays low spin during oxidation and reduction. *J. Biol. Chem.* 258:14908–14913.

37. Reference deleted in proof.

38. Yu, C. A., L. Yu, and T. E. King. 1973. Kinetics of electron transfer between cardiac cytochrome c_1 and c. *J. Biol. Chem.* 248:528–533.

39. Matcher, S. J., M. Cope, and D. T. Delpy. 1994. Use of the water absorption spectrum to quantify tissue chromophore concentration changes in near-infrared spectroscopy. *Phys. Med. Biol.* 39:177–196.

40. Yu, L., J. X. Xu, ..., C. A. Yu. 1987. Properties of bovine heart mitochondrial cytochrome b560. *J. Biol. Chem.* 262:1137–1143.